HTML ABSTRACT + LINKS

Instability of a rotating thread in a second immiscible liquid

J. Ashmore[a] and H. A. Stone
Division of Engineering and Applied Sciences, Harvard University, Cambridge, Massachusetts 02138

(Received 14 March 2003; accepted 29 September 2003; published online 20 November 2003)

We consider the surface-tension-driven instability of a cylindrical liquid column surrounded by a second liquid when the entire system is rotating. Our calculations are in the limit that the flows in both the liquid thread and the outer fluid are viscously dominated, and include the centripetal and Coriolis forces; the effect of the Coriolis force has not previously been studied in the case that the flows in both liquids are viscous. We present numerical results of a linear temporal stability analysis, and an analytical result valid in the large-Taylor-number limit. We also use the boundary-integral method to consider the evolution and instability of a finite cylindrical thread, which then relaxes when the rotation rate is reduced. These results are discussed in connection with recent experimental observations. © *2004 American Institute of Physics.* [DOI: 10.1063/1.1629127]

I. INTRODUCTION

The seminal work of Rayleigh[1] and Tomotika[2] established the characteristics of the instability of a cylinder of viscous liquid due to surface tension. Following on from this research, a number of studies have examined the effect on this instability of centripetal forces arising from rotation.[3–9] Many investigations have included consideration of Coriolis forces,[3–5,9,10] although the effect of the Coriolis force in the two-fluid problem in the viscous limit, which is the focus of this paper, has not been studied. Some of the published research has been motivated by the development of the spinning drop tensiometer by Vonnegut,[11] which is useful for making measurements of interfacial tension between two fluids.

Our study is motivated by recent experiments using a spinning drop tensiometer.[6] In these experiments, a cylindrical container is filled with two colloidal suspensions of different densities. When the tensiometer is rotated about its axis, the fluid of lower density aligns along the axis of rotation due to centripetal effects, forming a cylindrical thread. For sufficiently rapid rotation rates (described in terms of nondimensional parameters in the main body of the text), this configuration is stable and the equilibrium shape of the thread has been characterized analytically.[10,11] When the rotation rate is reduced below a critical value, the centripetal forces arising from rotation are too weak to suppress the capillary instability and a stationary instability grows until eventually the thread breaks into drops.

The experimental results generated with a spinning drop tensiometer can be used to determine the unknown surface tension between two fluids from the measured growth rate of the instability, as has been reported by de Hoog and Lekkerkerker.[6,12] Such a spinning drop method is advantageous when the surface tension is very small, as is often the case in colloidal systems; static measurement methods for measuring the interfacial tension in these liquid–liquid systems are difficult due to the long time necessary to equilibrate.[6] These studies have been based on a Newtonian constitutive equation for the fluids, which should provide a reasonably accurate description of colloidal systems when the flow is close to a rigid body motion so that elastic effects remain relatively weak.

This paper is organized as follows: we focus on the viscous limit and use a temporal linear stability analysis to consider the effect of the Coriolis force and of a rigid outer boundary on the predictions of the initial growth rate and most unstable wave number of the capillary instability. The linear stability analysis calculation in the quasistatic limit is presented in Sec. II A, and an analytic result that is asymptotically valid in the limit of large Taylor numbers is given in Sec. II B. Numerical results are discussed in Sec. III, and are compared with analytic results where possible. Finally, in Sec. IV we study the global shape change that occurs when a finite cylindrical thread, which is generated by rapid rotation of a container filled with two liquids of different densities, relaxes to a shorter and fatter equilibrium shape when the rotation rate is reduced. This sequence of changes in the rotation rate mimics the experimental protocol in recent work.[6,7,12] Our numerical results highlight one aspect of the experimental approach that may be influenced by the finite length of the elongated drop. We give conclusions in Sec. V, and Appendices A, B, and C include, respectively, calculations in the large-Taylor-number limit, of the effect of a rigid outer boundary, and with the quasistatic assumption relaxed.

II. LINEAR STABILITY ANALYSIS: PROBLEM FORMULATION

We consider the stability of a rotating cylindrical liquid thread of radius a surrounded by an outer fluid rotating at the same angular velocity Ω about the axis of the thread; buoyancy effects are assumed to be negligible. We work in rotating cylindrical coordinates (r,θ,z) and choose the z-axis of the coordinate system to coincide with the axis of rotation, as

[a]Present address: DAMTP, University of Cambridge, Wilberforce Road, Cambridge CB3 0WA, United Kingdom.

 © 2004 American Institute of Physics

Downloaded 23 Aug 2004 to 130.83.214.34. Redistribution subject to AIP license or copyright, see http://pof.aip.org/pof/copyright.jsp

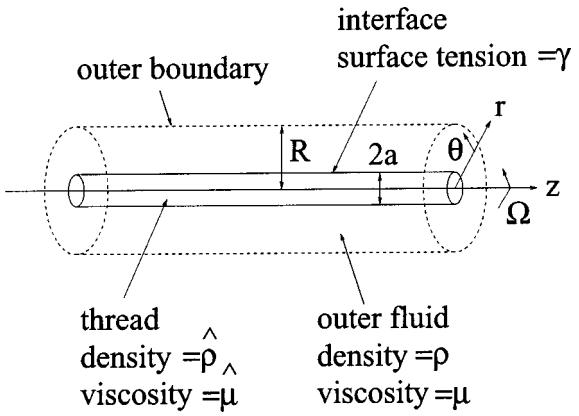

FIG. 1. Rotating thread of uniform radius a in a rotating outer fluid. The presence of an outer boundary at $r=R$ is shown. Note that most of the calculations exclude the effect of the outer boundary, but we discuss the effect of the outer boundary in Sec. III and Fig. 4.

indicated in Fig. 1. For the linear stability analysis we assume that the perturbations are independent of θ.

The thread radius is perturbed to $r=a(1+\epsilon(t)\cos kz)$, where k is real, and the equations governing the evolution of $\epsilon(t)$ are derived. The inner and outer fluid pressure and velocity perturbations are, respectively, denoted by $\hat{p}$, p, $\hat{\mathbf{u}}=(\hat{u}_r,\hat{u}_\theta,\hat{u}_z)$ and $\mathbf{u}=(u_r,u_\theta,u_z)$. Although the flow and shape are assumed to be independent of θ, swirl exists $(u_\theta,\hat{u}_\theta\neq 0)$ so that all fields depend on r, z, and time t only. The inner (outer) fluid has density $\hat{\rho}$ (ρ) and viscosity $\hat{\mu}$ (μ), and the interfacial tension between the two fluids is denoted by γ.

We nondimensionalize by scaling lengths by a, velocities by $u_c=\gamma/\mu$, and stresses by $\mu u_c/a=\gamma/a$. For the quasistatic two-fluid problem, which involves five material parameters $(\rho,\hat{\rho},\mu,\hat{\mu},\gamma)$, four dimensionless groups must be specified in general. These are the Taylor number $\mathcal{T}$, representing the ratio of Coriolis to viscous forces in the outer fluid, the rotational Bond number $\mathcal{B}_\Omega$, representing the ratio of centripetal to surface tension forces, the density ratio, and the viscosity ratio:

$$\mathcal{T}=\frac{2\rho\Omega a^2}{\mu},\quad \mathcal{B}_\Omega=\frac{(\rho-\hat{\rho})\Omega^2 a^3}{\gamma},\quad \frac{\hat{\rho}}{\rho},\quad \text{and}\ \frac{\hat{\mu}}{\mu}. \tag{1}$$

Including the effects of an outer boundary introduces a fifth dimensionless group, R/a, and including inertia introduces a Reynolds number (Appendix C).

Theoretically, the rotational Bond number $\mathcal{B}_\Omega$ may be either positive or negative, although when $\rho<\hat{\rho}$, so that $\mathcal{B}_\Omega<0$, the cylindrical thread is unstable at all rotation speeds. However, when the lower density fluid forms the thread and $\rho>\hat{\rho}$ $(\mathcal{B}_\Omega>0)$, the thread is stable at "high" rotation speeds when $\mathcal{B}_\Omega>1$ but is unstable otherwise. Therefore, below we consider the typical experimental protocol[12] such that a cylindrical thread is generated at a "high" rotation rate and following reduction of the rotation rate to a lower level, there is a capillary instability, which leads to breakup of the thread into small drops.

A. The quasistatic limit

The dimensional Navier–Stokes equations in a coordinate system rotating with angular velocity $\mathbf{\Omega}=\Omega\mathbf{e}_z$ can be written as[13,14]

$$\rho\left(\frac{\partial\mathbf{u}}{\partial t}+\mathbf{u}\cdot\nabla\mathbf{u}+2\mathbf{\Omega}\wedge\mathbf{u}\right)=-\nabla p_d+\mu\nabla^2\mathbf{u},\quad \nabla\cdot\mathbf{u}=0, \tag{2}$$

where the dynamic pressure p_d, neglecting gravitational buoyancy, and the fluid pressure p are related by $p_d=p+(\rho/2)(\mathbf{\Omega}\wedge\mathbf{x})^2$ (here $\mathbf{x}$ denotes the position vector). Equations for the interior fluid are distinguished by a $\hat{}$. We first consider the quasistatic limit and small Reynolds number $\hat{\rho}\gamma a/(\mu\hat{\mu})\ll 1$. Then, for the droplet phase the linearized equations, scaled as described at the end of the last section, are

$$\frac{\hat{\rho}}{\rho}\mathcal{T}\mathbf{e}_z\wedge\hat{\mathbf{u}}=-\nabla\hat{p}_d+\frac{\hat{\mu}}{\mu}\nabla^2\hat{\mathbf{u}},\quad \nabla\cdot\hat{\mathbf{u}}=0, \tag{3}$$

where we have chosen to maintain the same variables for their dimensionless counterparts. Here $\mathbf{e}_z$ denotes the unit vector in the z-direction. The centripetal term re-enters the problem when the normal stress balance is used, but it only modifies the "effective pressure." The equations for the outer fluid can be obtained from (3) by putting $\hat{\rho}/\rho=1$, $\hat{\mu}/\mu=1$, and then the quasistatic approximation requires $\rho\gamma a/\mu^2\ll 1$.

Assuming that the instability is axisymmetric and accounting for a swirling motion $(\hat{u}_\theta\neq 0)$, the governing equations in cylindrical coordinates for the interior flow are

$$\frac{\hat{\rho}}{\rho}\mathcal{T}\hat{u}_\theta=-\frac{\partial\hat{p}_d}{\partial r}+\frac{\hat{\mu}}{\mu}\left[\frac{\partial}{\partial r}\left(\frac{1}{r}\frac{\partial}{\partial r}(r\hat{u}_r)\right)+\frac{\partial^2\hat{u}_r}{\partial z^2}\right], \tag{4a}$$

$$-\frac{\hat{\rho}}{\rho}\mathcal{T}\hat{u}_r=\frac{\hat{\mu}}{\mu}\left[\frac{\partial}{\partial r}\left(\frac{1}{r}\frac{\partial}{\partial r}(r\hat{u}_\theta)\right)+\frac{\partial^2\hat{u}_\theta}{\partial z^2}\right], \tag{4b}$$

$$0=-\frac{\partial\hat{p}_d}{\partial z}+\frac{\hat{\mu}}{\mu}\left[\frac{1}{r}\frac{\partial}{\partial r}\left(r\frac{\partial\hat{u}_z}{\partial r}\right)+\frac{\partial^2\hat{u}_z}{\partial z^2}\right], \tag{4c}$$

$$0=\frac{1}{r}\frac{\partial}{\partial r}(r\hat{u}_r)+\frac{\partial\hat{u}_z}{\partial z}. \tag{4d}$$

For a shape $r=1+\epsilon(t)\cos(kz)$, we seek solutions consistent with $u_r\propto\cos kz$:

$$(\hat{\mathbf{u}},\hat{p})=\epsilon(t)(\cos(kz)\hat{U}_r(r),\cos(kz)\hat{U}_\theta(r),\sin(kz)\hat{U}_z(r),\cos(kz)\hat{P}(r)). \tag{5}$$

Substituting into (4) and combining the coupled ODEs that result, we obtain a sixth-order ODE for $\hat{U}_r(r)$

$$\left[\mathcal{L}^3-\left(k\frac{\hat{\rho}}{\rho}\frac{\mu}{\hat{\mu}}\mathcal{T}\right)^2\right]\hat{U}_r=0,$$

where

$$\mathcal{L}(g(\mathbf{x}))\equiv\frac{d}{dr}\left(\frac{1}{r}\frac{d}{dr}(rg)\right)-k^2g, \tag{6}$$

Downloaded 23 Aug 2004 to 130.83.214.34. Redistribution subject to AIP license or copyright, see http://pof.aip.org/pof/copyright.jsp

for a function $g(\mathbf{x})$. Setting $\hat{\rho}=\rho$, $\hat{\mu}=\mu$, we obtain $(\mathcal{L}^3-k^2\mathcal{T}^2)U_r=0$ for the exterior fluid. Equation (6) can be factored into the form

$$(\mathcal{L}-\hat{\alpha}_1)(\mathcal{L}-\hat{\alpha}_2)(\mathcal{L}-\hat{\alpha}_3)\hat{U}_r=0,$$

where

$$\hat{\alpha}_1=\left[k\frac{\hat{\rho}}{\rho}\frac{\mu}{\hat{\mu}}\mathcal{T}\right]^{2/3}, \quad \hat{\alpha}_{2,3}=-\left[k\frac{\hat{\rho}}{\rho}\frac{\mu}{\hat{\mu}}\mathcal{T}\right]^{2/3}\frac{(1\pm i\sqrt{3})}{2}. \quad (7)$$

For the exterior fluid the three roots $\{\alpha_j\}$ are $\alpha_1=(k\mathcal{T})^{2/3}$, $\alpha_{2,3}=-(k\mathcal{T})^{2/3}(1\pm i\sqrt{3})/2$.

The solutions to the second-order ODE of the form $(\mathcal{L}-\hat{\alpha})f=0$, where $\mathcal{L}$ is given in (6), are modified Bessel functions of order one of the first and second kind: $f(r)=\{I_1(r\sqrt{k^2+\hat{\alpha}}),K_1(r\sqrt{k^2+\hat{\alpha}})\}$. Then, the solutions internal and external to the thread, respectively, have the form

$$\hat{U}_r(r)=\sum_{j=1}^{3} a_j I_1(r\sqrt{k^2+\hat{\alpha}_j}),$$

$$U_r(r)=\sum_{j=1}^{3} b_j K_1(r\sqrt{k^2+\alpha_j}). \quad (8)$$

The other velocity components and the stresses follow by direct differentiation in accordance with (4) and (5). We have performed all of the necessary mathematical operations in the steps that follow using the Matlab software.

We now apply the six boundary conditions which thus determines a matrix equation for the six unknowns, $\{a_j,b_j\}$ with $j=1$, 2, 3. As is common in linear stability problems, although the interface lies at $r=1+\epsilon\cos kz$, the boundary conditions may be applied at $r=1$ to leading order in ϵ for $\epsilon\ll 1$. Continuity of velocity yields three equations,

$$\hat{\mathbf{u}}=\mathbf{u} \quad \text{at } r=1, \quad (9)$$

and another three conditions follow from continuity of tangential stress and the normal stress jump at $r=1$. The dimensionless stress condition is written in terms of the stress tensor $\mathbf{T}^d$ defined using the dynamic pressure. Also, $\mathbf{e}_r$ is the unit radial vector and approximates the unit normal to the interface $r=1+\epsilon\cos kz$. To leading order in ϵ the stress jump at the interface is

$$\mathbf{e}_r\cdot(\hat{\mathbf{T}}^d-\mathbf{T}^d)=(1-k^2-\mathcal{B}_\Omega)\epsilon(t)\cos(kz)\mathbf{e}_r \quad \text{at } r=1. \quad (10)$$

Note that in the normal stress component of (10), the familiar term $(1-k^2)$ accounts for the contribution of surface tension times curvature, and $\mathcal{B}_\Omega$ enters because the pressure is modified by centripetal effects. We have not written the constant reference pressure that balances the normal stress due to the curvature of the undeformed cylindrical shape.

The 6×6 matrix equation generated by substituting the velocity fields determined from (8) into (9) and (10) has the form $\mathbf{M}\cdot\mathbf{x}=\mathbf{c}$, where $\mathbf{x}$ is the vector of coefficients $\{a_j,b_j\}$. All entries of $\mathbf{c}$ are zero except for the "standard" one arising from the normal stress balance, which equals $(1-k^2-\mathcal{B}_\Omega)$. Hence we may think of this term as the "driving force" of the instability and we comment below on implications of the value of $\mathcal{B}_\Omega$ that can be deduced from the structure of this term.[1–6,8–10] The matrix equation is solved numerically to obtain the $\{a_j,b_j\}$ as a function of k, $\mathcal{T}$, $\hat{\rho}/\rho$, $\hat{\mu}/\mu$, and $\mathcal{B}_\Omega$.

With the $\{a_j\}$ known, the dimensionless growth rate σ, scaled by $\gamma/\mu a$, can be determined by writing $\epsilon(t)=\epsilon_0 e^{\sigma t}$, consistent with the form of the linear stability equation, which for the interface $r=1+\epsilon(t)\cos kz$ yields

$$\frac{\partial r}{\partial t}=\hat{u}_r|_{r=1}\Rightarrow\sigma=\sum_{j=1}^{3} a_j I_1(\sqrt{k^2+\hat{\alpha}_j}). \quad (11)$$

Clearly, $\Re(\sigma)>0$ implies instability and $\Re(\sigma)<0$ implies stability. As we have used complex functions in the general expressions for $\hat{U}_r(r)$ and $U_r(r)$ [see (8)], the constants a_j, b_j are complex, although we find that the pressure and velocity fields are all real, as expected. The growth rate σ is also real and so the instability is stationary.

Tomotika[2] studied the two-fluid thread stability problem in the absence of rotation, i.e., $\mathcal{T}=0$, $\mathcal{B}_\Omega=0$, and we have verified that our results reproduce Tomotika's in this limit. Relative to other linear stability papers in the literature ours is the first to include Coriolis effects in the dynamics of the two-fluid problem in the viscous limit, although a number of other studies have included Coriolis effects when considering a liquid cylinder in a gas[3–5,9] and when considering a bubble surrounded by a liquid in the inviscid limit.[10]

B. Large-Taylor-number asymptotics

When either the inner and/or outer Taylor numbers become large, a boundary layer is introduced where viscous terms are important close to the interface between the two fluids but are negligible far away. We focus on the case that both the inner and outer Taylor numbers are large, $\mu\hat{\rho}\mathcal{T}/(\hat{\mu}\rho)\gg 1$, $\mathcal{T}\gg 1$. Because of the form of Eq. (6), the boundary layers scale with the one-third power of the appropriate Taylor number. The details of the calculation are given in Appendix A. For the growth rate σ we find

$$\sigma=f\left(\frac{\hat{\rho}}{\rho},\frac{\hat{\mu}}{\mu}\right)\frac{k(1-k^2-\mathcal{B}_\Omega)}{\mathcal{T}}, \quad (12)$$

where in general the function f has many terms. Equation (12) can be rewritten in the form

$$\frac{\sigma\mathcal{T}}{(1-\mathcal{B}_\Omega)^{3/2}}=f\left(\frac{\hat{\rho}}{\rho},\frac{\hat{\mu}}{\mu}\right)K(1-K^2),$$

where

$$K=\frac{k}{(1-\mathcal{B}_\Omega)^{1/2}}, \quad (13)$$

which isolates the effect of the Bond number. The most unstable wave number is then found to be independent of $\hat{\rho}/\rho$, $\hat{\mu}/\mu$, and $\mathcal{T}$, with the value $k_{\text{crit}}=\sqrt{(1-\mathcal{B}_\Omega)/3}$. The corresponding maximum growth rate is

$$\sigma_{\max}=\frac{2(1-\mathcal{B}_\Omega)^{3/2}}{3\sqrt{3}\mathcal{T}}f\left(\frac{\hat{\rho}}{\rho},\frac{\hat{\mu}}{\mu}\right).$$

Also, in the limit $\hat{\mu}/\mu=1$, we find

Downloaded 23 Aug 2004 to 130.83.214.34. Redistribution subject to AIP license or copyright, see http://pof.aip.org/pof/copyright.jsp

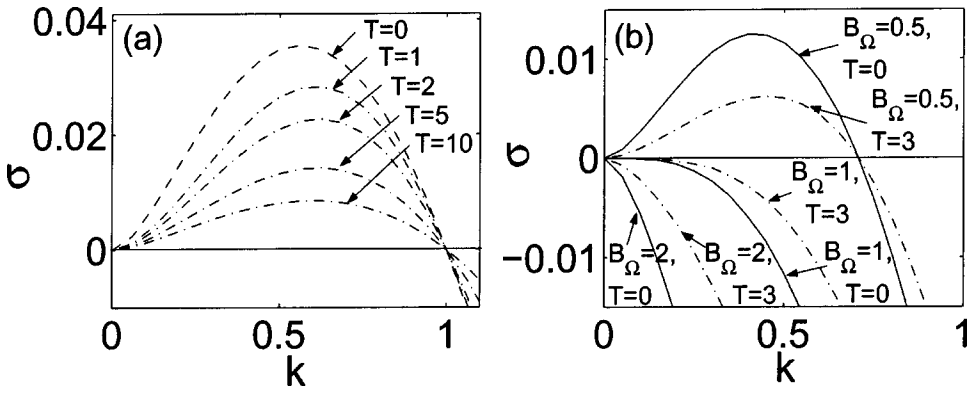

FIG. 2. (a) Stability diagram for $\hat{\mu}/\mu=1$, $\hat{\rho}/\rho=1$ and $\mathcal{B}_\Omega=0$, showing the effect of the Coriolis force in the absence of centripetal effects. All calculations are based on the quasistatic approximation. The growth rate σ has been nondimensionalized by $\gamma/\mu a$ and k has been nondimensionalized by $1/a$. The dashed line, $\mathcal{T}=0$, is the zero rotation result (Ref. 2). (b) The effect of the Coriolis force (choosing $\mathcal{T}=3$) for different values of the rotational Bond number $\mathcal{B}_\Omega$, with $\hat{\mu}/\mu=1$ and $\hat{\rho}/\rho=0.5$. When $0<\mathcal{B}_\Omega\leqslant 1$ and there is a range of unstable wave numbers, rotation does not alter the stability of a disturbance with a particular wave number, but reduces the maximum growth rate. Note that when $\mathcal{B}_\Omega=0.5$, the small wave numbers remain unstable, when $\mathcal{B}_\Omega=1$, the small wave numbers are neutrally stable and when $\mathcal{B}_\Omega=2$, the small wave numbers are stable.

$$f\left(\frac{\hat{\rho}}{\rho},1\right)=\frac{1}{[1+(\hat{\rho}/\rho)^{1/3}][1+(\hat{\rho}/\rho)^{1/3}+(\hat{\rho}/\rho)^{2/3}]}. \qquad (14)$$

The asymptotic predictions for the growth rates and critical wave numbers are compared with numerical results in Sec. III.

III. LINEAR STABILITY ANALYSIS: NUMERICAL RESULTS

In this section we examine how the Coriolis and centripetal forces affect the familiar capillary instability that occurs at small wave numbers $0<k<1$ in the absence of rotation.[1,2,15] We also examine when the effect of an outer boundary is significant in suppressing the instability, and consider the results obtained when the quasistatic approximation is relaxed.

The importance of centripetal effects is indicated by the value of the rotational Bond number $\mathcal{B}_\Omega$, which appears in the only nonzero term $(1-k^2-\mathcal{B}_\Omega)$ on the right-hand side of the matrix equation for the coefficients, e.g., see (10). As mentioned earlier, when $\mathcal{B}_\Omega<0$, i.e., $\rho<\hat{\rho}$, a stable thread can never be formed and therefore we do not consider this case. When $0<\mathcal{B}_\Omega<1$, centripetal effects suppress the capillary instability, i.e., for the unstable small wave numbers, $0<k<\sqrt{1-\mathcal{B}_\Omega}$, the growth rate is reduced. These wave numbers nevertheless remain unstable. Finally, when $\mathcal{B}_\Omega>1$, centripetal effects stabilize the small wave numbers and since large wave numbers are stabilized by surface tension, all wave numbers are stable. Therefore when $\mathcal{T}=0$ and as the rotational Bond number increases through positive values, both the range of unstable wave numbers and the maximum growth rate decrease. The centripetal effect has been well studied for the case $\mathcal{T}=0$ and is a natural modification to Tomotika's original result for the two-fluid capillary instability.

We examine the influence of the Coriolis force in the absence of centripetal effects. Thus, we take $\hat{\mu}/\mu=1$ and $\hat{\rho}/\rho=1$ so that $\mathcal{B}_\Omega=0$. The growth rate σ as a function of the wave number k for different $\mathcal{T}$ is plotted in Fig. 2(a), which shows that the Coriolis force is stabilizing in the sense that the maximum growth rate decreases and the most unstable wave number increases (i.e., wavelength decreases) as the Taylor number $\mathcal{T}$ increases. The reduction in the growth rate is consistent with the qualitative trend of the asymptotic result in the large-Taylor-number limit, which shows that $\sigma\approx(1-\mathcal{B}_\Omega)^{3/2}/\mathcal{T}$ when $\mathcal{T}\gg 1$ [see Eq. (13)]. The growth rate for nonzero Bond number, i.e., when the centripetal force is nonzero, for $\mathcal{T}=0$ and $\mathcal{T}=3$ is plotted in Fig. 2(b) ($\hat{\rho}/\rho=0.5$). In general, larger values of both the Bond number $\mathcal{B}_\Omega$ and the Taylor number $\mathcal{T}$ lead to a reduction in the maximum growth rate.

We next make a quantitative comparison between the asymptotic and numerical results from the linear stability theory for the growth rate and critical wave number of the instability, focusing on larger values of the Taylor number so that the nondimensional boundary layer width $\mathcal{T}^{-1/3}$ is small as required. In Fig. 3(a) we compare the theoretical prediction (12) for the growth rate with numerical results from the linear stability calculation. We work in the limit $\hat{\mu}/\mu=1$ so that the function f in (12) is given by (14). The growth rate and wave number have been rescaled as in (13) to facilitate easy comparison, although multiplying the growth rate σ by Taylor number $\mathcal{T}$ exaggerates the discrepancy between numerical and theoretical results for large Taylor numbers. The comparison is in fact quite reasonable when $\mathcal{T}^{-1/3}\ll 1$.

To understand the reduction in the growth rate from a physical point of view, consider a radial perturbation to the base state.[9,13] A radial velocity $u_r\mathbf{e}_r$ induces a Coriolis force proportional to $\mathbf{\Omega}\wedge\mathbf{u}=\Omega u_r\mathbf{e}_\theta$, and this azimuthal force will lead to an increase in the azimuthal velocity. Representing the additional azimuthal velocity by $u_\theta\mathbf{e}_\theta$, this in turn will lead to a Coriolis force proportional to $\mathbf{\Omega}\wedge\mathbf{u}=-\Omega u_\theta\mathbf{e}_r$, i.e., a force opposing the radial growth. Therefore the growth rate is reduced, which is consistent with the trends shown in Fig. 2.

Next we show in Fig. 3(b) the critical wave number as a function of the rotational Bond number for large Taylor numbers. The most unstable wave number decreases from a

Downloaded 23 Aug 2004 to 130.83.214.34. Redistribution subject to AIP license or copyright, see http://pof.aip.org/pof/copyright.jsp

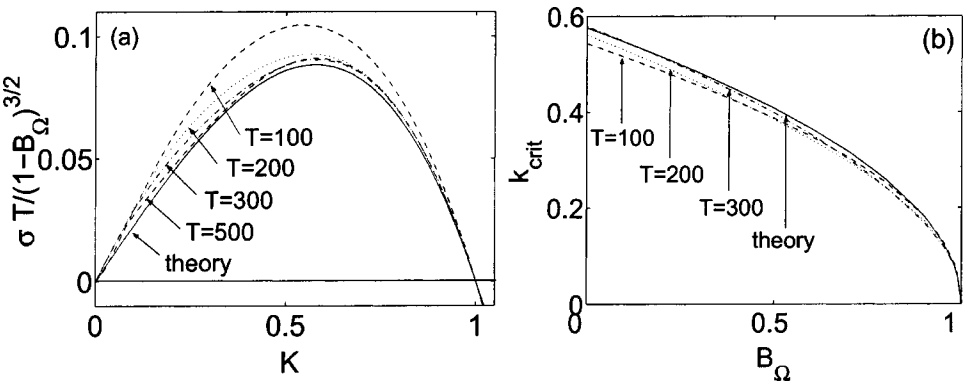

FIG. 3. (a) A plot of the rescaled growth rate $\sigma\mathcal{T}/(1-\mathcal{B}_\Omega)^{3/2}$ against the rescaled wave number $K=k/(1-\mathcal{B}_\Omega)^{1/2}$, showing the theoretical prediction in the large-Taylor-number limit using the function f given in (14) and numerical results with $\hat{\rho}/\rho=0.5$ and $\hat{\mu}/\mu=1$. Curves for different values of the Bond number $\mathcal{B}_\Omega=0$, 0.5 but the same value of the Taylor number $\mathcal{T}$ are indistinguishable. (b) The critical wave number, corresponding to the maximum linear growth rate, as a function of rotational Bond number $\mathcal{B}_\Omega$ for Taylor number $\mathcal{T}=100$, 200, 300 and $\hat{\mu}/\mu=1$, $\hat{\rho}/\rho=0.5$. Also plotted is the theoretical prediction for the critical wave number derived from large-Taylor-number asymptotics $k_{\text{crit}}=\sqrt{(1-\mathcal{B}_\Omega)/3}$ (see Sec. II B). All calculations are in the quasistatic limit.

maximum value of approximately 0.58 when $\mathcal{B}_\Omega=0$ to zero when $\mathcal{B}_\Omega=1$, but is only weakly dependent on the Taylor number. Physically, the dominant mechanism in determining the critical wave number is competition between centripetal forces (which act to reduce the critical wave number) and surface tension forces (which increase the critical wave number), and the Coriolis acceleration has little effect. The asymptotic prediction for wave number $k_{\text{crit}}=\sqrt{(1-\mathcal{B}_\Omega)/3}$, valid when $\mathcal{T}\gg 1$, is plotted in Fig. 3(b) and is seen to be in quite reasonable agreement with the numerical results when $\mathcal{T}^{-1/3}\ll 1$.

We also examine the effect of an outer boundary on the stability of the thread. The modifications to the analysis are described in Appendix B. On physical grounds, we expect that a nearby rigid boundary suppresses the instability and this is consistent with the variation of growth rate versus wave number shown in Fig. 4. When $R/a=2$, the effect of geometrical confinement is strong and the dispersion relationships for $\mathcal{T}=0$, 1, 3 are indistinguishable. Also, the critical wave number increases as the boundary approaches the interface between the thread and the outer fluid. The numerical results, though, indicate that the effect is less than 10% when $R/a>5$.

In Appendix C, the calculation of the growth rate is described when the quasistatic approximation is not used. In the case the importance of inertia due to unsteadiness relative to viscous effects is measured by a Reynolds number $\mathrm{Re}=\rho\gamma a/\mu^2=(1-\hat{\rho}/\rho)\mathcal{T}^2/(4\mathcal{B}_\Omega)$. The real growth rate determined from theory with and without the quasistatic approximation when $\mathrm{Re}=10$, 100 are plotted in Fig. 4(b). When $\mathrm{Re}=100$, the deviation between the two sets of results reaches a maximum of 22%.

The theoretical analysis described in this section has shown that the Coriolis force and the presence of an outer boundary affect the growth rate and wavelength of an instability. Using representative experimental values for colloidal solutions[12] of $\rho-\hat{\rho}=2\times10^{-4}\,\mathrm{g/cm^3}$, $\mu=1$ Poise, $\Omega=600$ rad/s, $a=0.015\,\mathrm{cm}$, $\gamma=2\times10^{-3}\,\mathrm{dyn/cm}$, the Taylor number $\mathcal{T}=0.2$. A larger thread radius a, for example, will result in an increase in the Taylor number $\mathcal{T}$. Therefore it is worth keep-

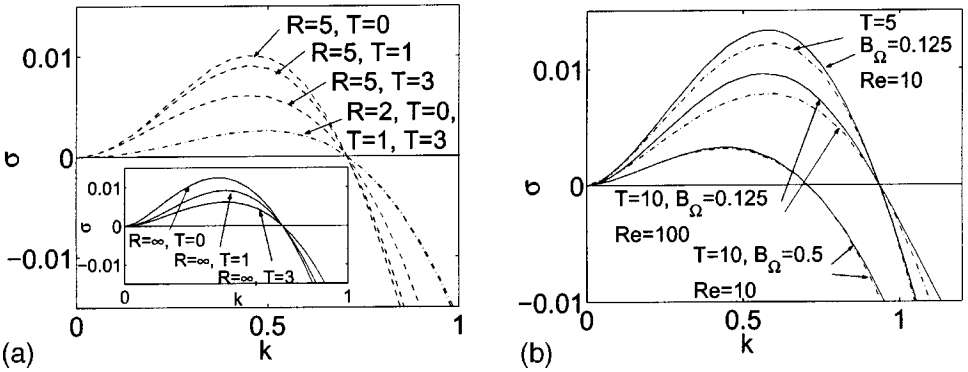

FIG. 4. (a) The effect of an outer boundary on the instability. All data are for $\hat{\mu}/\mu=1$, $\hat{\rho}/\rho=0.5$, $\mathcal{B}_\Omega=0.5$ and are calculated in the quasistatic limit. These results show that when R/a becomes small, the instability is damped by the boundary. (b) A plot of results from the theory based on the quasistatic approximation and with the quasistatic approximation relaxed, for two different values of the Reynolds number. The dotted–dashed lines are the results from theory using the quasistatic approximation, and the solid lines are results from theory with this assumption relaxed, including the time derivative terms. $\hat{\rho}/\rho=0.5$ and $\hat{\mu}/\mu=1$ in all cases. For $\mathcal{B}_\Omega=0.125$, $\mathcal{T}=10$, and the Reynolds number $\mathrm{Re}=(1-\hat{\rho}/\rho)\mathcal{T}^2/(4\mathcal{B}_\Omega)=100$ (see Appendix C), and for both pairs of values $\mathcal{B}_\Omega=0.5$, $\mathcal{T}=10$ and $\mathcal{B}_\Omega=0.125$, $\mathcal{T}=5$, $\mathrm{Re}=10$. Note that the difference between the results from theory with and without the quasistatic approximation when $\mathrm{Re}=10$ is substantially greater when $\mathcal{B}_\Omega=0.125$, $\mathcal{T}=5$ than when $\mathcal{B}_\Omega=0.5$, $\mathcal{T}=10$.

Downloaded 23 Aug 2004 to 130.83.214.34. Redistribution subject to AIP license or copyright, see http://pof.aip.org/pof/copyright.jsp

ing the influence of Coriolis effects in mind, especially if experiments involve even smaller density differences since in such cases increases in the thread radius a or rotation rate Ω, which maintain $\mathcal{B}_\Omega$ constant, will also lead to larger Taylor numbers.

It is interesting to consider the above results in light of the experimental data of de Hoog and Lekkerkerker.[6] In general, these authors found excellent agreement between their experimental measurements and the predictions of a linear stability theory with $\mathcal{T}=0$. Nevertheless, de Hoog and Lekkerkerker find that the experimentally measured growth rate is about 1.5 times larger than the prediction of linear stability analysis [Fig. 6(a) of Ref. 6]. Since in the experiments $\mathcal{T}\approx 1$ (based on the second lower rotation rate) and $R/a \geqslant 13$, both Coriolis effects and the presence of an outer boundary are negligible. Also, our analysis has shown that accounting for Coriolis effects or the presence of an outer boundary lead to a reduction in the growth rate predicted by linear stability theory, whereas in the experiments the observed growth rate was larger than the theoretically predicted value. Therefore the discrepancy must be accounted for by another mechanism. In the next section, we consider retraction of the ends of the threads arising from the reduction in rotation rate, and the subsequent uniform radial growth, as a possible explanation for the small discrepancy between experiment and theory.

IV. NUMERICAL SIMULATION OF THE EVOLUTION OF A FINITE THREAD

We now consider a second aspect of fluid motion that may impact the experimentally observed growth rate on a fluid thread of finite length:[6] When the rotation rate is reduced from its initial value at which the thread is stable to the lower rate at which the thread is unstable, then, in addition to the development of the local instability, there is a global change of shape as the thread relaxes towards its equilibrium shape at the lower rotation rate. In particular, the ends of the thread retract and the average radius of the thread increases, since the equilibrium shape of the thread at the lower final rotation rate is relatively short and fat compared to the equilibrium shape at the initial higher rotation rate.[10,11] Any such relaxation-driven increase in the thread radius would impact interpretation of the growth rate of an instability observed by experimental measurements of the thread radius versus time. In this section, we use a numerical simulation based on the boundary-integral method to examine the evolution of the thread. This approach accounts for centripetal effects but not Coriolis effects, and incorporates the effect of the finite thread length and the flow that accompanies relaxation.

The dimensional time scale over which a transient solution lasts when the rotation rate of the container is reduced by an amount $\Delta\Omega$ may be estimated by the viscous time scale $\rho R^2/\mu$, where R is the cylinder radius, or the Ekman time scale associated with spin-down[14] $\sqrt{\rho L^2/(\mu\Delta\Omega)}$, where L is the length of the cylindrical container. Using representative experimental values[12] of $\rho=1$ g/cm^3, $R=0.2$ cm, $L=4$ cm, $\mu=1$ Poise, $\Delta\Omega=540$ rad/s, $a=0.015$ cm, $\gamma=2\times10^{-3}$ dyn/cm, the Ekman time scale is longer than the viscous timescale and we use this as a conservative estimate of the time scale over which the transient exists. Nondimensionalizing using the time scale $\mu a/\gamma$, the nondimensional Ekman spin-down time is approximately 2.3×10^{-2}, which is much smaller than the time scales we consider here. Therefore we neglect the effects of the transient solution associated with the spin-down process.

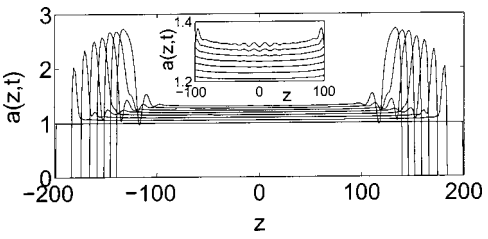

FIG. 5. A numerical solution generated using the boundary-integral method for $\mathcal{B}_\Omega=0.15$, $\hat{\mu}/\mu=1$ and initial aspect ratio 1:200. The curves are for nondimensional times $t=0$, 100, 200, 300, 400, 500, 600, 700 and the initial shape is a cylindrical thread with hemispherical ends. The inset shows the onset of the instability in the central section.

Both the boundary-integral formulation, which neglects the Coriolis force, and the numerical method are standard.[16] Using the nondimensional variables defined in Sec. II, the equation for the interfacial velocity is

$$\frac{1}{2}\left(1+\frac{\hat{\mu}}{\mu}\right)\mathbf{u}(\mathbf{x}_s)+\left(1-\frac{\hat{\mu}}{\mu}\right)\int_{S(t)}\mathbf{n}\cdot\mathbf{K}\cdot\mathbf{u}\,dS_y = -\int_{S(t)}\left[\nabla_s\cdot\mathbf{n}+\frac{\mathcal{B}_\Omega}{2}|\mathbf{\Omega}\wedge\mathbf{y}|^2\right]\mathbf{n}\cdot\mathbf{J}\,dS_y, \tag{15}$$

where $S(t)$ is the surface of the thread, $\mathbf{x}_s$ lies on $S(t)$, dS_y is the scalar area element at point $\mathbf{y}$, and the kernel functions are

$$\mathbf{J}(\mathbf{r})=\frac{1}{8\pi}\left[\frac{\mathbf{I}}{r}+\frac{\mathbf{rr}}{r^3}\right],\quad \mathbf{K}(\mathbf{r})=-\frac{3}{4\pi}\frac{\mathbf{rrr}}{r^5},\quad \mathbf{r}=\mathbf{x}-\mathbf{y}. \tag{16}$$

The unit normal $\mathbf{n}$ and the vector $\mathbf{y}$ are of the form

$$\mathbf{n}=\left(\cos\theta,\sin\theta,-\frac{\partial a}{\partial z}\right)\left[1+\left(\frac{\partial a}{\partial z}\right)^2\right]^{-1/2}, \tag{17a}$$

$$\mathbf{y}=(a(z,t)\cos\theta,a(z,t)\sin\theta,z), \tag{17b}$$

where θ is the azimuthal angle and $a(z,t)$ denotes the radial coordinate of the interface. We have limited our investigation to $\hat{\mu}/\mu=1$, which simplifies considerably the numerical work, but still allows us to identify a possibly important physical aspect of experimental measurements.

We note that when comparing with the typical experimental protocol in which the liquid thread is generated at a higher rotation rate and then the instability is induced by reducing the rotation rate, the Bond number that appears in the calculations of this section is based on the lower rotation rate. The initial (high) rotation rate only sets the initial shape of the drop used in the simulation.

We first consider the relaxation of the shape of a thread for an initial aspect ratio (defined as the diameter divided by

Downloaded 23 Aug 2004 to 130.83.214.34. Redistribution subject to AIP license or copyright, see http://pof.aip.org/pof/copyright.jsp

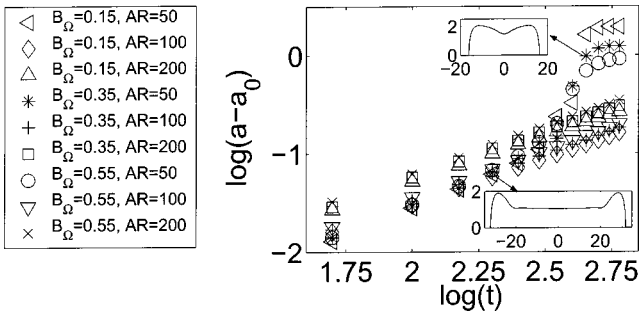

FIG. 6. The average radius, defined by taking the average of the central peak and trough, as a function of time. Averaging in this way removes the contribution of the local instability to growth. a_0 is the initial radius and AR denotes the initial aspect ratio. The insets show typical thread shapes, $a(z,t)$ vs z, for $\mathcal{B}_\Omega=0.35$ and initial aspect ratio 50, with arrows indicating the data point corresponding to the plot.

the length) of 1/200, with $\mathcal{B}_\Omega=0.15$ and $\hat{\mu}/\mu=1$. The numerical simulations shown in Fig. 5 exhibit significant growth of the radius with time at the center of the thread and at later times an instability begins to evolve on top of this radial growth (see inset). The large droplets developing at the ends of the thread will eventually break off; however this process has been found to have little effect on the dynamics of the remaining thread.[17] Thus we expect that the observed growth rate found from experimental measurements of the change of radius with time comprise contributions due to the average radial growth of the thread as well as the natural instability of the cylindrical shape, and should be compared to predictions of theory that accounts for both of these growth processes. In the analysis that follows we consider separately the average radial growth rate and the growth rate of the oscillatory perturbation to the interface.

We next report the results for several different initial thread aspect ratios and Bond numbers and, in Figs. 6 and 7, respectively, plot the average increase in radius and the decrease in thread length $\ell(t)$ as a function of time (here a_0 and ℓ_0 denote, respectively, the initial radius and length of the thread). For both quantities the time derivative seems to be approximately constant up to a certain maximum time when the rate of increase of the radius is more rapid as the two ends meet: this can be observed for the curves with initial aspect ratio 50 in the inset of Fig. 6. It would be interesting to derive a theoretical prediction of the rate of change of the thread radius and length; however, we have not succeeded with such a calculation. The evolution of the thread involves the development of two bulbous ends as the thread shortens, and a small amount of fluid leaks out of the bulbous ends into the main body of the thread and is distributed evenly. Some models have characterized the growth of bulbous ends when viscous effects are unimportant,[18,19] but it has not yet been possible to generalize these to the viscously dominated limit; e.g., other studies of the retraction of films have been limited to numerical methods only.[20]

For sufficiently large initial aspect ratios, we can compare the wave number and growth rate of the interfacial instability obtained from the boundary-integral code with the predictions of the linear stability analysis. Taking $\mathcal{B}_\Omega=0.15$ and $\hat{\mu}/\mu=1$ with an initial aspect ratio of 1:200, the radial growth rate, which includes both uniform radial growth and the developing instability, is $\sigma_{\text{full}}=\dot{a}(t)/a(t)$, where the dot denotes the derivative with respect to time. We find $\sigma_{\text{full}}\approx 0.92$; in the range of times considered here the fractional incarease in a is sufficiently small that the growth rate σ_{full}, which account for the dynamics associated with the finite length of the thread, is always large compared to the linear instability growth rate. The corresponding nondimensional wave number is $k=0.39$. To focus on the instability, we subtract off the average radial growth rate which yields the nondimensional growth rate $\sigma=0.017$. A comparison of σ with the result of the linear stability calculation with the same value of $\mathcal{B}_\Omega$ and $\hat{\mu}/\mu$ and $\mathcal{T}=0$ was not favorable: the linear stability calculation predicted a maximum nondimensional growth rate $\sigma=0.028$ and a nondimensional critical wave number $k_{\text{crit}}=0.52$. However, as can be seen from the numerical results of the boundary-integral code in Fig. 5, there is uniform radial growth before the onset of the instability and therefore the relevant value of the Bond number $\mathcal{B}_\Omega$, which is proportional to the cube of the radius, for the instability is larger than the initial value used in the boundary-integral code: if the onset of instability occurs when the thread radius is a_1, the effective Bond number at that instant is $\mathcal{B}_\Omega(a_1/a_0)^3$ and it is this value that should be used in the linear stability calculation. In the particular case considered, $a_1/a_0=1.3$ and the effective Bond number at the onset of instability is 0.33; using this value in the linear stability calculation gives a maximum growth rate $\sigma=0.020$ and a critical wave number $k_{\text{crit}}=0.46$, which is in better agreement with the boundary-integral results. The remaining small discrepancy may arise due to the effect of modifications of the internal and external velocity fields that accompany relaxation of the finite thread.

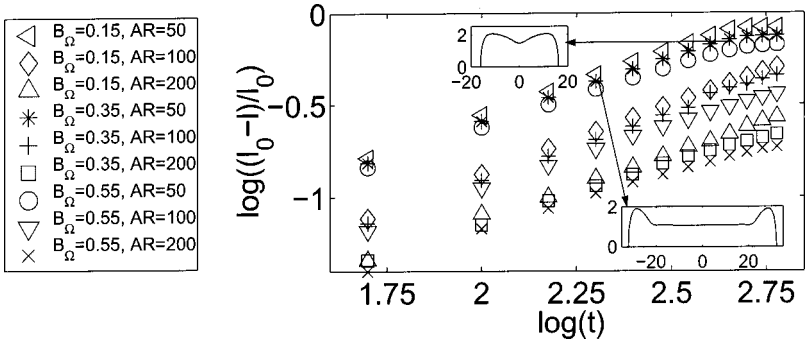

FIG. 7. A plot of the thread length ℓ as a function of time. $\hat{\mu}/\mu=1$ and ℓ_0 denotes the initial length. The insets show the thread shape [radius $a(z,t)$ plotted against axial coordinate z] for the times indicated by the arrows.

Downloaded 23 Aug 2004 to 130.83.214.34. Redistribution subject to AIP license or copyright, see http://pof.aip.org/pof/copyright.jsp

As remarked earlier, in the work of de Hoog and Lekkerkerker[6] linear stability theory underestimated the experimentally observed growth rate. This trend is consistent with the numerical results given here which show that uniform radial thickening of the thread can contribute to an increased apparent growth rate. However, we have insufficient information to know whether this is the true explanation for the experimental observations of these authors where there is some discrepancy between experimental results and predictions of linear stability theory. It may be of interest to be aware of this dynamical possibility in future experiments using the spinning drop tensiometer to determine a value of the interfacial tension by a thread breakup experiment.

V. CONCLUDING REMARKS

We have used analytical and numerical methods based on a linear temporal stability analysis to study the effect of rotation on the classical surface-tension-driven Rayleigh instability of a cylindrical liquid column. The effect of the Coriolis force is to suppress the maximum growth rate of the instability, and we have determined asymptotic results for the growth rate and the critical wave number in the limit $\mathcal{T}\gg 1$. We have also considered the presence of a rigid outer boundary and have compared numerical results obtained from analysis with and without use of the quasistatic approximation.

Although the Coriolis force may in general be important, its contribution does not explain the small discrepancy between theory, which accounts for the centripetal force but not the Coriolis force, and experimental measurements of the growth rate in the work of de Hoog and Lekkerkerker.[6] Therefore we have studied numerically the radial growth of the thread that is initially generated at a high rotation rate but which relaxes to a shorter and fatter shape after the rotation rate is reduced. The growth rates predicted by the linear stability calculation and the boundary-integral results were in reasonable agreement after accounting for the uniform increase in radius of the finite thread before the onset of instability.

ACKNOWLEDGMENTS

We gratefully acknowledge useful discussions with H. N. W. Lekkerkerker, and financial support from the Harvard MRSEC and PPG Industries Inc.

APPENDIX A: LARGE-TAYLOR-NUMBER ASYMPTOTICS

Without rescaling variables it would appear that the viscous terms in Eqs. (4a)–(4d) are negligible; however, a solution in which viscous terms are not included cannot satisfy the normal stress boundary condition (10). In the case that $\mathcal{T}\gg 1$ and $\mu\hat{\rho}\mathcal{T}/(\hat{\mu}\rho)\gg 1$ there are two boundary layers, one on either side of the interface. Therefore, we rescale r inside by $r=1-\hat{R}(\hat{\mu}\rho/(\mu\hat{\rho}\mathcal{T}))^{1/3}$ and rescale r outside by $r=1+R/\mathcal{T}^{1/3}$, where the one-third scaling is motivated by the form of Eq. (6). Then, for $\mathcal{T}\gg 1$ and using the form for the pressure and velocity field given by (5), the equations governing the radial velocity component outside the thread are approximated as

$$(\mathcal{L}^3-(k\mathcal{T})^2)U_r=0\Rightarrow\left(\frac{d^6}{dR^6}-k^2\right)U_r=0, \tag{A1}$$

with errors $O(\mathcal{T}^{-1/3})$. This equation has the solution

$$\begin{aligned}U_r=&c_1e^{-k^{1/3}R}+e^{-(k^{1/3}R/2)}\left[c_2\cos\left(\frac{\sqrt{3}}{2}k^{1/3}R\right)\right.\\&\left.+c_3\sin\left(\frac{\sqrt{3}}{2}k^{1/3}R\right)\right]+c_4e^{k^{1/3}R}\\&+e^{(k^{1/3}R/2)}\left[c_5\cos\left(\frac{\sqrt{3}}{2}k^{1/3}R\right)+c_6\sin\left(\frac{\sqrt{3}}{2}k^{1/3}R\right)\right],\end{aligned} \tag{A2}$$

where c_1, c_2, c_3, c_4, c_5, and c_6 are constants to be determined. Since the velocity field is bounded as $R\to\infty$, then $c_4=c_5=c_6=0$. The pressure field and axial and azimuthal velocity components follow from the governing equations [see (4a)–(4d)]:

$$P=-\frac{\mathcal{T}^{2/3}}{k}\frac{d^2U_z}{dR^2}+O(1), \tag{A3a}$$

$$U_z=-\frac{\mathcal{T}^{1/3}}{k}\frac{dU_r}{dR}+O(1), \tag{A3b}$$

$$U_\theta=-\frac{1}{\mathcal{T}^{2/3}}\frac{dP}{dR}+O\left(\frac{1}{\mathcal{T}^{1/3}}\right). \tag{A3c}$$

A similar approach for $\mu\hat{\rho}\mathcal{T}/(\hat{\mu}\rho)\gg 1$ based on the rescaling for $\hat{R}$ inside the thread, with the requirement the solutions decay as $\hat{R}\to\infty$, leads to the general solution

$$\begin{aligned}\hat{U}_r=&c_7e^{-k^{1/3}\hat{R}}+e^{-(k^{1/3}\hat{R}/2)}\left[c_8\cos\left(\frac{\sqrt{3}}{2}k^{1/3}\hat{R}\right)\right.\\&\left.+c_9\sin\left(\frac{\sqrt{3}}{2}k^{1/3}\hat{R}\right)\right],\end{aligned} \tag{A4}$$

where c_7, c_8, and c_9 are constants that are to be determined. The pressure and azimuthal and axial velocity fields are again determined from equations analogous to (4a)–(4d), which are similar to (A3) but have some differences in signs since $\partial/\partial r$ is equivalent to $-(\mu\hat{\rho}\mathcal{T}/(\hat{\mu}\rho))^{1/3}\partial/\partial\hat{R}$ rather than $\mathcal{T}^{1/3}\partial/\partial R$ and also involve extra factors of $\mu/\hat{\mu}$ and $\hat{\rho}/\rho$.

The six boundary conditions at the interface $r=1$, i.e., $R=0$, $\hat{R}=0$ yield six equations for the constants c_1, c_2, c_3, c_7, c_8, and c_9. Solving these equations symbolically (using Matlab) gives a theoretical prediction of the growth rate σ

$$\sigma=c_1+c_2=f\left(\frac{\hat{\rho}}{\rho},\frac{\hat{\mu}}{\mu}\right)\frac{k(1-k^2-\mathcal{B}_\Omega)}{\mathcal{T}}, \tag{A5}$$

where in general the function f has many terms. An expression for f in the limit $\hat{\mu}/\mu=1$ is given in (14), and the criti-

Downloaded 23 Aug 2004 to 130.83.214.34. Redistribution subject to AIP license or copyright, see http://pof.aip.org/pof/copyright.jsp

cal wave number is also given in Sec. II B. The predictions of growth rate and critical wave number are compared with numerical results in Sec. III.

APPENDIX B: THE PRESENCE OF A RIGID OUTER BOUNDARY

The above analysis is easily modified to take account of a rigid boundary at radial distance $R>a$. We use the quasistatic approximation, and modify the analysis of Sec. II A. The expression for the inner radial velocity in (8) remains the same, but the general expression for the outer radial velocity becomes

$$U_r(r)=\sum_{j=1}^{3} b_j K_1(r\sqrt{k^2+\alpha_j})+\sum_{j=4}^{6} b_j I_1(r\sqrt{k^2+\alpha_j}). \tag{B1}$$

We must now solve for the nine constants $\{a_j,b_j\}$. In addition to the three velocity boundary equations and three stress boundary conditions on the interface at $r=1$ [see Eqs. (9) and (10)], there are three no-slip velocity boundary conditions $\mathbf{u}=\mathbf{0}$ to be applied at $r=R/a$. The details of this calculation were implemented in a straightforward manner using Matlab software.

APPENDIX C: RELAXING THE ASSUMPTION OF QUASISTATIC FLOW

In deriving (3) from the Navier–Stokes equations (2) we have assumed that the velocity field is quasistatic, i.e., that the velocity changes on a sufficiently slow time scale that the time derivative term $\partial\mathbf{u}/\partial t$ may be neglected. We now describe how the above linear stability calculation is altered when this assumption is relaxed.

Above we have nondimensionalized time with the scale $\mu a/\gamma$. Retaining the time-derivative term in the governing equations leads to the introduction of the Reynolds number $\mathrm{Re}=\rho\gamma a/\mu^2=(1-\hat{\rho}/\rho)\mathcal{T}^2/(4\mathcal{B}_\Omega)$, which is often referred to as the Ohnesorge number. Then the analog of Eqs. (4a)–(4c) for the interior flow is

$$\frac{\hat{\rho}}{\rho}\left(\mathrm{Re}\frac{\partial\hat{u}_r}{\partial t}+\mathcal{T}\hat{u}_\theta\right) = -\frac{\partial\hat{p}_d}{\partial r}+\frac{\hat{\mu}}{\mu}\left[\frac{\partial}{\partial r}\left(\frac{1}{r}\frac{\partial}{\partial r}(r\hat{u}_r)\right)+\frac{\partial^2\hat{u}_r}{\partial z^2}\right], \tag{C1a}$$

$$\frac{\hat{\rho}}{\rho}\left(\mathrm{Re}\frac{\partial\hat{u}_\theta}{\partial t}-\mathcal{T}\hat{u}_r\right)=\frac{\hat{\mu}}{\mu}\left[\frac{\partial}{\partial r}\left(\frac{1}{r}\frac{\partial}{\partial r}(r\hat{u}_\theta)\right)+\frac{\partial^2\hat{u}_\theta}{\partial z^2}\right], \tag{C1b}$$

$$\frac{\hat{\rho}}{\rho}\mathrm{Re}\frac{\partial\hat{u}_z}{\partial t}=-\frac{\partial\hat{p}_d}{\partial z}+\frac{\hat{\mu}}{\mu}\left[\frac{1}{r}\frac{\partial}{\partial r}\left(r\frac{\partial\hat{u}_z}{\partial r}\right)+\frac{\partial^2\hat{u}_z}{\partial z^2}\right], \tag{C1c}$$

$$0=\frac{1}{r}\frac{\partial}{\partial r}(r\hat{u}_r)+\frac{\partial\hat{u}_z}{\partial z}, \tag{C1d}$$

with similar equations for the exterior flow. Again, we assume the flow field (5) and it can be shown that the equation for the radial velocity $\hat{U}_r$, analogous to (6), is

$$\left[\left(\mathcal{L}-\mathrm{Re}\frac{\hat{\rho}\mu}{\rho\hat{\mu}}\frac{1}{\epsilon}\frac{d\epsilon}{dt}\right)^3+\mathrm{Re}\frac{\hat{\rho}\mu}{\rho\hat{\mu}}\frac{1}{\epsilon}\frac{d\epsilon}{dt}\left(\mathcal{L}-\mathrm{Re}\frac{\hat{\rho}\mu}{\rho\hat{\mu}}\frac{1}{\epsilon}\frac{d\epsilon}{dt}\right)^2 -\left(k\frac{\hat{\rho}\mu}{\rho\hat{\mu}}\mathcal{T}\right)^2\right]\hat{U}_r=0. \tag{C2}$$

Now the roots $\{\hat{\alpha}_i\}$ with $i=1, 2, 3$, defined in (7), and also the roots $\{\alpha_i\}$ and coefficients $\{a_i,b_i\}$ in the solution forms (8), are dependent on the unknown growth rate σ. Since the right-hand side of (11) is now a function of σ, the growth rate is determined by using a standard root-finding program to determine the value of the growth rate σ such that

$$\sum_{j=1}^{3} a_j(\sigma)I_1(\sqrt{k^2+\hat{\alpha}_j(\sigma)})-\sigma=0, \tag{C3}$$

where the coefficients $a_j(\sigma)$ and $\hat{\alpha}_j(\sigma)$ are calculated numerically for a given value of σ. To find the root σ, we use the Matlab routine "fzero," which uses a combination of bisection, secant and inverse quadratic interpolation. We also plotted the left-hand side of (C3) as a function of σ for fixed wave number k, which established the uniqueness of the solution. Although it is possible that with the quasistatic approximation relaxed there may be complex growth rates which are solutions to (C3), due to the difficulty in calculating the complex solutions we have considered only real solutions. The results of this calculation are discussed in Sec. III.

[1] Lord Rayleigh, "On the instability of a cylinder of viscous liquid under the capillary force," Philos. Mag. **34**, 145 (1892).
[2] S. Tomotika, "On the instability of a cylindrical thread of a viscous liquid surrounded by another viscous fluid," Proc. R. Soc. London, Ser. A **150**, 322 (1935).
[3] J. Eggers and M. P. Brenner, "Spinning jets," in *Proceedings of the IUTAM Symposium on Nonlinear Waves in MultiPhase Flow*, edited by H.-C. Chang (Kluwer, Dordrecht, 2000).
[4] J. Gillis and B. Kaufman, "The stability of a rotating viscous jet," Q. Appl. Math. **19**, 301 (1961).
[5] L. M. Hocking, "The stability of a rigidly rotating column of liquid," Mathematika **7**, 1 (1960).
[6] E. H. A. de Hoog and H. N. W. Lekkerkerker, "Breakup of an elongated droplet in a centrifugal field," J. Phys. Chem. B **105**, 11636 (2001).
[7] H. N. W. Lekkerkerker and E. H. A. de Hoog, "The break-up of a liquid cylinder in a centrifugal field," Physica A **298**, 69 (2001).
[8] T. J. Pedley, "Stability of rotating with a cylindrical free surface," J. Fluid Mech. **30**, 127 (1967).
[9] D. F. Rutland and G. J. Jameson, "Droplet production by the disintegration of rotating liquid jets," Chem. Eng. Sci. **25**, 1301 (1970).
[10] D. K. Rosenthal, "The shape and stability of a bubble at the axis of a rotating liquid," J. Fluid Mech. **12**, 358 (1962).
[11] B. Vonnegut, "Rotating bubble method for the determination of surface and interfacial tension," Rev. Sci. Instrum. **13**, 6 (1942).
[12] E. H. A. de Hoog and H. N. W. Lekkerkerker, "Measurement of the interfacial tension of a phase-separated colloid-polymer suspension," J. Phys. Chem. B **103**, 5274 (1999).
[13] G. K. Batchelor, *An Introduction to Fluid Dynamics* (Cambridge University Press, Cambridge, 1967).
[14] H. P. Greenspan, *The Theory of Rotating Fluids* (Breukelen, Brookline, 1990).

Downloaded 23 Aug 2004 to 130.83.214.34. Redistribution subject to AIP license or copyright, see http://pof.aip.org/pof/copyright.jsp

[15]S. Chandrasekhar, *Hydrodynamic and Hydromagnetic Stability* (Oxford University Press, Oxford, 1961).
[16]J. R. Lister and H. A. Stone, ''Time-dependent viscous deformation of a drop in a rapidly rotating denser fluid,'' J. Fluid Mech. **317**, 275 (1996).
[17]M. Tjahjadi, H. A. Stone, and J. M. Ottino, ''Satellite and subsatellite formation in capillary breakup,'' J. Fluid Mech. **243**, 297 (1992).
[18]J. B. Keller, ''Breaking of liquid films and threads,'' Phys. Fluids **26**, 3451 (1983).
[19]J. B. Keller, A. King, and L. Ting, ''Blob formation,'' Phys. Fluids **7**, 226 (1995).
[20]M. P. Brenner and D. Gueyffier, ''On the bursting of viscous films,'' Phys. Fluids **11**, 737 (1999).

Downloaded 23 Aug 2004 to 130.83.214.34. Redistribution subject to AIP license or copyright, see http://pof.aip.org/pof/copyright.jsp